X-ray structure of an anti-fungal chitosanase from *streptomyces* N174

Edward M. Marcotte[1], Arthur F. Monzingo[1], Stephen R. Ernst[1], Ryszard Brzezinski[2] and Jon D. Robertus[1]

We report the 2.4 Å X-ray crystal structure of a protein with chitosan endo-hydrolase activity isolated from *Streptomyces* N174. The structure was solved using phases acquired by SIRAS from a two-site methyl mercury derivative combined with solvent flattening and non-crystallographic two-fold symmetry averaging, and refined to an *R*-factor of 18.5%. The mostly α-helical fold reveals a structural core shared with several classes of lysozyme and barley endochitinase, in spite of a lack of shared sequence. Based on this structural similarity we postulate a putative active site, mechanism of action and mode of substrate recognition. It appears that Glu 22 acts as an acid and Asp 40 serves as a general base to activate a water molecule for an S_N2 attack on the glycosidic bond. A series of amino-acid side chains and backbone carbonyl groups may bind the polycationic chitosan substrate in a deep electronegative binding cleft.

[1]Department of Chemistry and Biochemistry University of Texas Austin, Texas 78712, USA
[2]Groupe de Recherche en Biologie des Actinomyctes Département de Biologie, Faculté des Sciences, Université de Sherbrooke, Sherbrooke, Qubec, J1K 2R1, Canada

Correspondence should be addressed to J.D.R.

Chitosan, a linear polysaccharide of β-(1,4)-linked D-glucosamine residues, has diverse commercial applications, ranging from bioerodeable suture material and drug delivery systems to metal removal from waste streams[1]. Although manufactured industrially by deacetylation of chitin, chitosan is a naturally occurring component of fungal cell walls. It appears primarily in a group of medically and agriculturally significant fungi, the *Zygomycetes.* These include opportunistic invaders of humans and major pathogens in burn wounds[2], as well as important agricultural pathogens. In some *Mucor* species, chitosan can account for as much as 30% of the dry weight of the cell wall[3]. Interestingly, chitosan oligomers inhibit the growth of a variety of fungal species[4]. In addition, chitosan oligomers induce disease response genes, such as endo-chitinase and endo-β-glucanase, in many plant species including pea, tomato and wheat[5].

An estimated 1–7% of heterotrophic soil bacteria, as well as certain plants and fungi, express protein chitosanases capable of degrading chitosan[6]. Multiple chitosanase forms have been found in several plant species, where they are believed to aid in the defense against invading fungal pathogens by destroying the integrity of their cell walls[7]. In addition to direct destruction of fungal cell walls, chitosinases have other anti-fungal effects—for example, the production of chitosan oligomers. These bring to bear their own fungistatic effects, as well as increasing recruitment of other anti-fungal proteins to the area by activation of plant disease response genes.

The *Streptomyces* N174 chitosanase is a 238 amino-acid protein that represents up to 60% of the extracellular protein produced by strain N174. Naturally occurring chitosans often have a small fraction of N-acetylated residues, and N174 chitosanase hydrolyses chitosans of 1–60% acetylation in an endo fashion. N174 chitosanase shows no hydrolysis of two closely related polysaccharides[8]: chitin (fully acetylated chitosan) and carboxymethylcellulose (CM-cellulose) which differs from chitosan in having a hydroxyl, rather than amine, substituent on the sugar C2 position, as well as having an acetylated O6 group. Unlike other sugar-cleaving enzymes that often hydrolyse chitosan to some extent, the chitosanases are the only enzymes active against fully deacetylated chitosan[8]. The N174 enzyme has been cloned and expressed to very high levels in *Streptomyces lividans*[9,10], making it amenable to biophysical analyses. Initial examinations of the protein sequence led us to believe that this chitosanase was homologous only with a chitosanase (glycosyl hydrolase family 46; ref. 11) from *Bacillus circulans*[12], and not with other sugar-cleaving enzymes. Our interest in the mechanism of chitosanase's precise specificity and its potential relationship to other sugar-cleaving enzymes led us to solve the enzyme's structure.

SIRAS phasing and model statistics

The crystallization of the protein was reported earlier[13]. The initial solvent-flattened SIRAS 3.0 Å map allowed identification of boundaries for the two molecules of the asymmetric unit. Averaging across the non-crystallographic two-fold symmetry axis produced an electron density map of sufficient quality to build most of the two molecules. This model had a crystallographic *R*-factor of 37%. After 22 rounds of crystallographic refinement, the *R*-factor is 18.1% at 2.4 Å resolution (R_{free}=23.6%, $R_{working}$=17.5%, where R_{free} represents 10% of the data) with 51 water

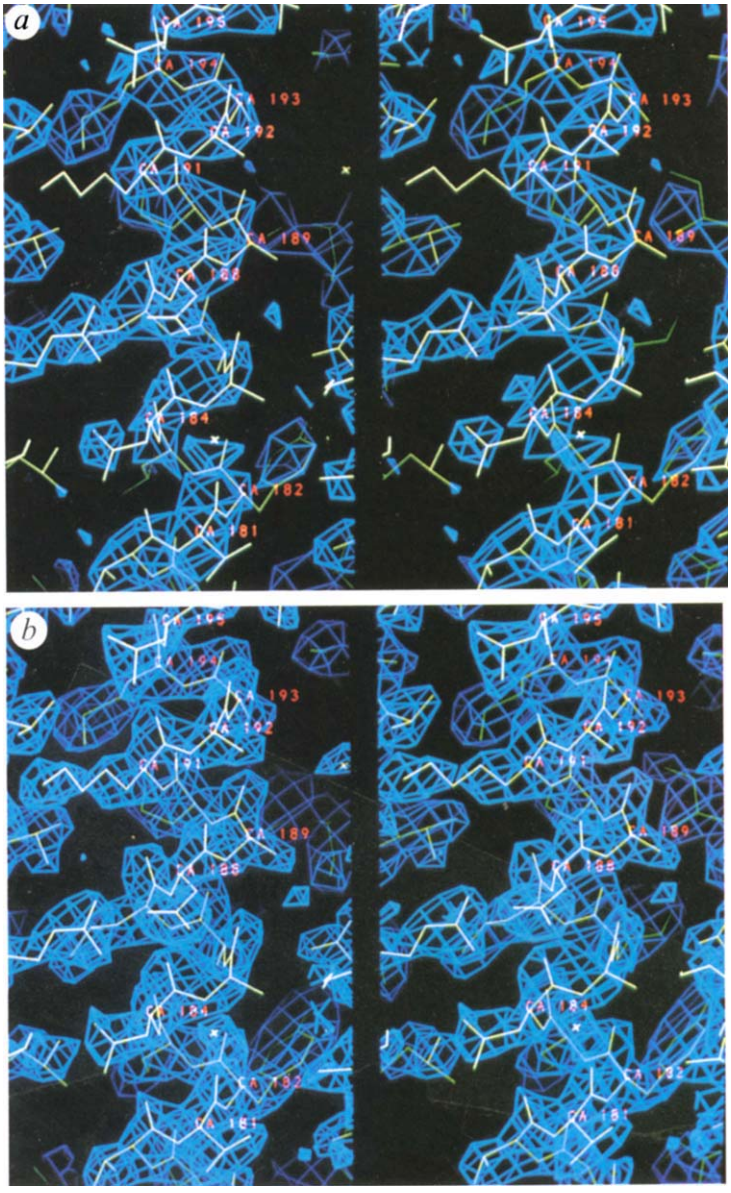

Fig. 1 *a*, A sample of the original 3.0 Å SIRAS solvent-flattened electron density map, displayed with the final model (residues 122–134) superimposed, is compared with *b*, the final 2.4 Å $2F_o$-F_c electron density map for this region. The electron density maps are contoured at 1.5 σ.

molecules included in the final model. The quality of the final $2F_o$-F_c map is shown in Fig. 1.

The final model, consisting of the entirety of both molecules in the crystallographic asymmetric unit, deviates from ideal bond lengths with an r.m.s. deviation of 0.016 Å and from ideal bond angles with an r.m.s. deviation of 3.118°. No residues lie in disallowed Ramachandran regions. For convenience, we refer to the two molecules of the asymmetric unit as a and b.

The approximate non-crystallographic two-fold axis was initially difficult to refine, and is distorted from ideality by asymmetric crystal contacts between residues 176–195 of molecule a with residues 22–40, 198–202 and 230–232 of a crystallographically related molecule b. The two molecules of the asymmetric unit can be aligned with an r.m.s. deviation of 0.8 Å for backbone atoms and 1.2 Å for all non-hydrogen atoms. The molecules are essentially identical in fold except for residues 198–202 (Fig. 2). These residues are involved in the asymmetric crystal contacts in molecule b and are in non-equivalent environments in the two molecules. This immediate region also receives low Eisenberg-Bowie 3D-1D scores[14], suggesting non-standard conformation whereas the rest of the model has reasonably high scores (overall scores are 107.0 for molecule a and 109.2 for molecule b, reasonable for proteins of this size). However, the region comprising residues 198–202 is a surface loop bordering the putative active site of the molecule—a site likely to be mobile in the absence of substrate. Electron density for amino acids 198–202 is poor, so this region was ultimately built using OMIT maps calculated from models that had undergone a round of simulated annealing with the residues removed to minimize model bias from the OMIT phases. In this paper, all analyses were performed with molecule a.

Structure of N174 chitosanase

The chitosanase molecule (Fig. 3) is dumbbell-shaped and ~55 Å long, containing two globular domains connected through a bent 27-residue backbone helix. The domains form a pronounced cleft, 10 Å wide and 12 Å deep, spanning the width of the molecule between the two domains. The cleft is bordered on one face by a three-stranded β-sheet. The molecule contains 10 α-helices, which compose 64% of the structure. Table 1 lists the secondary structure elements determined from hydrogen- bonding patterns and protein backbone φ–ψ angles observed in the chitosanase structure.

During the solution of the chitosanase structure, we noted a similarity to the structure of bacteriophage T4 lysozyme[15] (T4L). Although the two proteins share essentially no sequence homology, they have a roughly similar three-dimensional topology. The 74 residues of chitosinase, which have no structural correlates in T4L, are found in surface loops and insertions (Fig. 4). In fact, only about 45% of the amino acids in chitosanase can be considered to be in regions structurally equivalent to regions of T4L. When these 106 equivalent residues are considered in a structurally based sequence alignment, the identity is only 13%. T4L is also known to be structurally homologous to hen egg white lysozyme[16,17] (HEWL) and goose egg white lysozyme[18] (GEWL). Previously, we solved the X-ray structure of a barley endochitinase[19], and a similar structural homology to the lysozyme family has been found[20,21]. In short, this hydrolase superfamily can be divided on the basis of shared structural motifs into prokaryotic and eukaryotic families sharing a conserved core. Both families contain the structurally invariant core but have differing N- and C-terminal domains. The active sites of these enzymes can be aligned, and this equivalence has allowed us to form hypotheses about the minimal sugar-cleaving enzymatic unit as well as hypotheses about the chitosanase enzyme and its mode of action. A complete descrip-

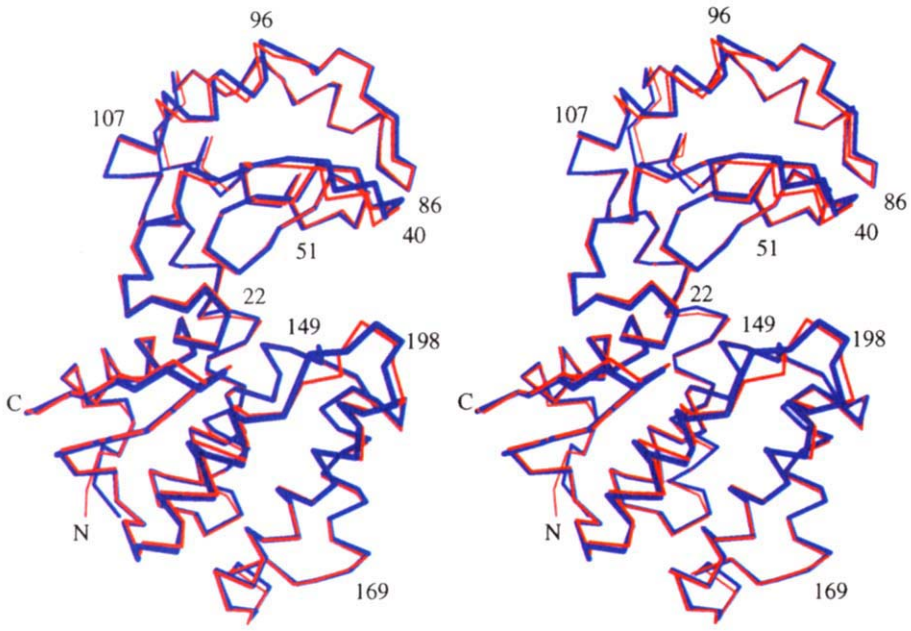

Fig. 2 A least-squares superposition of the two molecules of the chitosanase asymmetric unit. The molecules differ significantly only at residues 198–202. Molecule a is shown in bold blue lines; molecule b is shown in thin red lines. Only α-carbons are shown.

tion of the similarities between chitosanase, chitinase and lysozymes is presented in an accompanying manuscript[22].

Modelling of chitosan binding

In an attempt to directly study substrate binding, native crystals of wild-type chitosanase were soaked with chitosan monomers through tetramers. In no case was electron density attributable to chitosan found in difference Fourier electron density maps (data not shown). In the absence of crystallographic observation of a chitosanase–substrate complex, substrate binding was modelled by taking advantage of the structural homology of chitosanase to lysozymes, which have previously been co-crystallized with substrate[23,24]. Given the apparent structural similarity between chitosanase and lysozyme, it is reasonable to assume that polysaccharide substrates are bound in a similar fashion. Chitosans are chemically similar to the peptidoglycan attacked by lysozymes and the chitin attacked by chitinase, but they differ in being polycationic, as compared with the anionic lysozyme substrate or neutral chitinase substrate. Fig. 5 shows the charge distribution in the active-site cleft of chitosanase and chitinase. The surface of chitosanase is dominated by the electronegative substrate binding cleft, appropriate for binding a positively charged substrate. By comparison, the analogous cleft of chitinase is considerably more neutral. In all, at least 12 carboxylates contribute to the electronegative cleft of chitosanase (residues 22, 36, 37, 40, 57, 60, 117, 155, 197, 201, 202 and 232).

Aligning chitosanase with HEWL[25,26] and its crystallographically determined substrate analogues[23,24] suggests an initial model for chitosanase's substrate binding and specificity. Substrate binding in T4L and HEWL is mediated primarily by hydrogen bonding between the enzyme and substrate, and even involves contacts between peptide-bond heteroatoms and the saccharide substituents[27]. Six subsites are present in the HEWL active-site cleft for binding of up to six monosaccharide units of a poly-(N-acetylglucosamine-N-acetylmuramic acid) substrate (abbreviated NAG-NAM). These pockets are labelled A–F from the sugar nonreducing end, with catalysis occurring at the glycosidic bond linking sugars bound in the D and E sites.

Model building suggests barley chitinase also may form similar hydrogen bonds with the chitin substrate[21]. Model building of hexaglucosamine (chitosan) bound to the putative chitosanase active site suggests that substrate binding and the catalytic mechanism may be similar to these other glycohydrolases. Six sugar binding sites (A–F) can be identified in a fashion similar to lysozyme, with cleavage probably

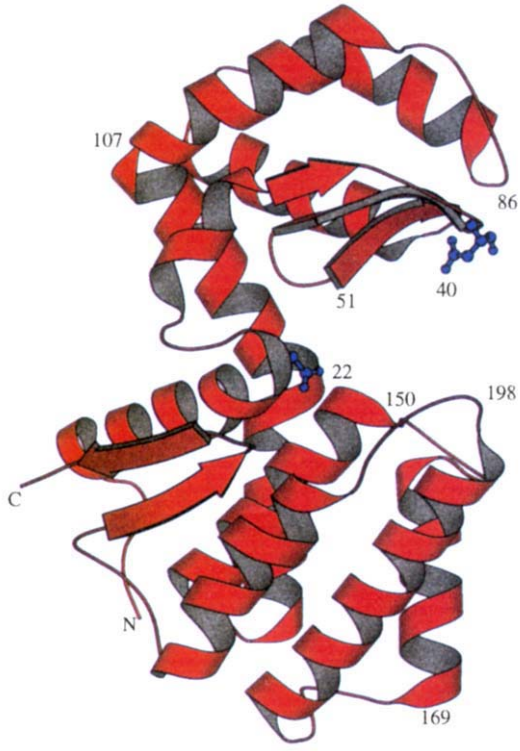

Fig. 3 A ribbon representation of the X-ray structure of *Streptomyces* N174 chitosanase. The putative active-site cleft is visible on the right side of the model. The side chain of the putative catalytic acids Glu 22 and Asp 40 are shown in blue bonds. Ribbon diagrams were produced using the program MOLSCRIPT[51].

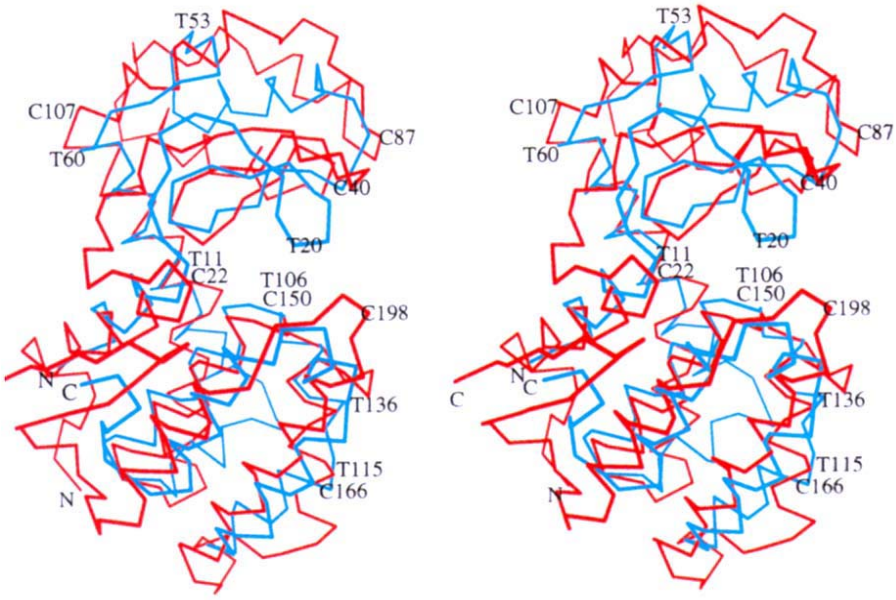

Fig. 4 A superposition of N174 chitosanase (red) and T4 lysozyme (cyan), displayed as a divergent stereo pair. Molecules are oriented as in Fig. 3; only α-carbons are drawn. Residues of chitosanase are labelled with the prefix C, those of T4L with the prefix T. In spite of the low sequence identity, an overall topological similarity can be observed.

This model of binding provides one explanation for chitosanase's inability to cleave chitin: N-acetyl groups would face steric crowding in sites A, B, C and D. Chitosanase's inability to cleave CM-cellulose may stem from steric crowding between the O-acetyl groups and side chains in the D, E, and F sites. The model does not prohibit catalysis of cellulose, but predicts reduced recognition of the uncharged substrate. Hydrogen bonds formed between protein carboxylates and cellulose are probably weaker than the corresponding ion pairs formed, in the desolvated cleft, with chitosan. Therefore, catalysis of cellulose, while not ruled out by the structure, may occur at levels lower than those of chitosan.

Chitosan hydrolysis

The similarities discussed in the previous section between the binding pockets of HEWL and chitosanase may initially suggest that the catalytic mechanisms of the two enzymes are similar: this is not the case. For HEWL, Glu 35 is believed to act as a general acid protonating the glycosidic oxygen between sugars D occurring at the glycosidic bond between the D and E sugars. Fig. 6 shows a schematic representation of bonding between chitosanase and hexaglucosamine in an energy-minimized model. Several enzyme–substrate hydrogen bonds are made that are not specific for the polysaccharide chitosan. Bonds from Arg 120, Asp 57, Tyr 122, Ile 49 and Asp 201 are found to chitosan sugar O6, O4 and O3 groups and could possibly be formed with common glucose derivatives. The model building suggests that chitosanase's preference for chitosan is mediated by bonding to the amines of sugars bound in sites A, B, C and D. Glu 60 may form an ion pair with the A sugar amine. The Pro 152 backbone carbonyl forms a hydrogen bond to the B sugar amine. Asp 57 forms an ion pair with the C sugar amine, while the backbone carbonyl oxygen of Gly 50 and possibly of Ile 49 may hydrogen bond to that group. Glu 197 may form an ion pair with the D sugar amine. Few enzyme–substrate interactions are noted for the putative E and F sites. Asp 201 may interact with O6 of the F sugar. The hydroxyl group of Tyr 34 is positioned 4.9 Å in our model from the amine of the E sugar and could interact if binding-induced conformational change occurs to bring it closer.

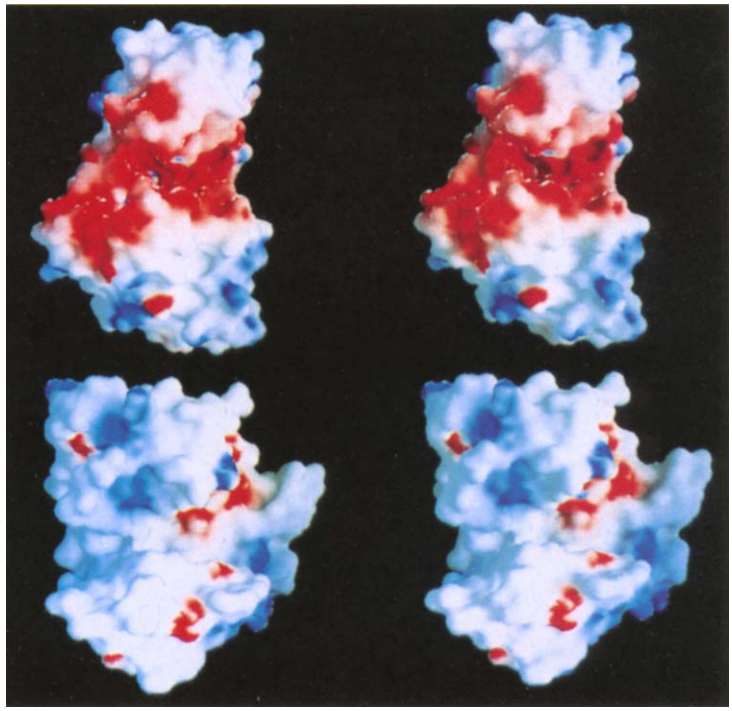

Fig. 5 Stereo diagram of molecular surface renderings of chitosanase (top) and barley chitinase (bottom). Surfaces are colored according to their electrostatic potentials as calculated by the program GRASP[50]. The surface potential is displayed as a color gradient from red (electronegative) to blue (electropositive), showing the relatively strong electronegative character of the putative active site cleft of chitosanase as compared to chitinase.

Table 1 Secondary structure of N174 chitosanase

Residues	Observed secondary structure
7–23	α-helix
28–33	α-helix
34–36	β-strand
42–47	β-strand
50–54	β-strand
56–69	α-helix
74–85	α-helix
94–107	α-helix
107–125	α-helix
125–134	α-helix
136–150	α-helix
158–170	α-helix
178–197	α-helix
203–217	α-helix
225–229	β-strand
232–236	β-strand

and E. A second carboxylate, Asp 52, is located to potentially afford stabilization of a putative resultant oxocarbonium ion intermediate[28,29]. The completion of the reaction occurs by attack on the oxocarbonium ion by a water molecule which replaces the E sugar when the product leaves. The reaction described is S_N1 and results in retention of the sugar's anomeric configuration (β); HEWL is thus classified as a retaining glycosidase. An alternative mechanism invokes a transient covalent intermediate between Asp 52 and the D sugar. Such a covalent intermediate has been trapped in the case of another retaining glycosidase, β-glucosidase, using 2-fluoro sugar derivatives[30] (reviewed in ref. 31).

A number of glycohydrolases proceed by an inverting mechanism. It has been suggested that unlike HEWL, T4 lysozyme may be an inverting enzyme[32]. Chitinase from yam has recently been shown to invert the β-anomeric form of the substrate into an α-anomer product[33], and this has been suggested as a possible mechanism for barley chitinase[21]. In an inverting enzyme, the glycosidic bond, and therefore the leaving (E) sugar, is protonated by a carboxylic acid. This protonation is accompanied by an attack from water on the opposite face of the D sugar.

The X-ray structure of *Streptomyces* chitosanase suggests that it is likely to be an inverting enzyme, with Glu 22 as the acid and Asp 40 as a base to polarize the attacking water molecule. The distance between the two active site carboxylates of glycohydrolases has been correlated with retaining and inverting mechanisms[34,35]. The distance between chitosanase Glu 22 and Asp 40 (13.8 Å in the apoenzyme, 12 Å in the enzyme–substrate model) corresponds more closely to what is observed in inverting β-glycosidases (~9.5 Å) than that of retaining β-glycosidases (~5 Å). Our substrate model has room between Asp 40 and the α face of sugar D to accomodate an attacking water molecule.

In our static model, it is difficult to position the substrate so that Glu 22 is hydrogen bonding to the D–E glycosidic oxygen while the Asp 40–H_2O–C1 (of sugar D) network also form strong hydrogen bonds. Although the geometry is good, the putative hydrogen-bond distance is long. The binding of substrate must alter the conformation of chitosanase somewhat to bring these key groups closer together. It is likely that Asp 40 on the β sheet loop is most mobile, while Glu 22 is probably fixed on the long central helix. Examination of the loops containing Asp 40 of chitosanase and Asp 22 of T4L (Fig. 4) shows the conformational variability of this loop between related glycohydrolase structures and reveals a potential movement of the chitosanase loop.

A likely mechanism for chitosanase hydrolysis is by a single displacement reaction mechanism (Fig. 7). Asp 40 is well positioned to act as a base and activate a water molecule to attack the D sugar's C1 carbon from the α side of the sugar. Because of steric hindrance by the D sugar ring's *peri* hydrogens (not drawn), it is likely that the D sugar must distort to a half-chair configuration to allow the proposed nucleophilic attack to proceed. This substrate distortion has been crystallographically observed in mutant T4L–substrate complexes[32], as well as in HEWL–substrate complexes (modeled by Imoto *et al.*[26]), HEWL–tetrasaccharide lactone inhibitor complexes[24] and mutant HEWL–substrate complexes[36], although this distortion was not seen in a recent GEWL–trisaccharide complex[37]. Glu 22 may help to promote the attack, serving to protonate the leaving group E sugar from the β side. The reaction proceeds until only di- and tri-glucosamines remain, with trace amounts of free D-glucosamine, suggesting that the minimal substrate is the tetrasaccharide[8], with low levels of hydrolysis of the trisaccharide.

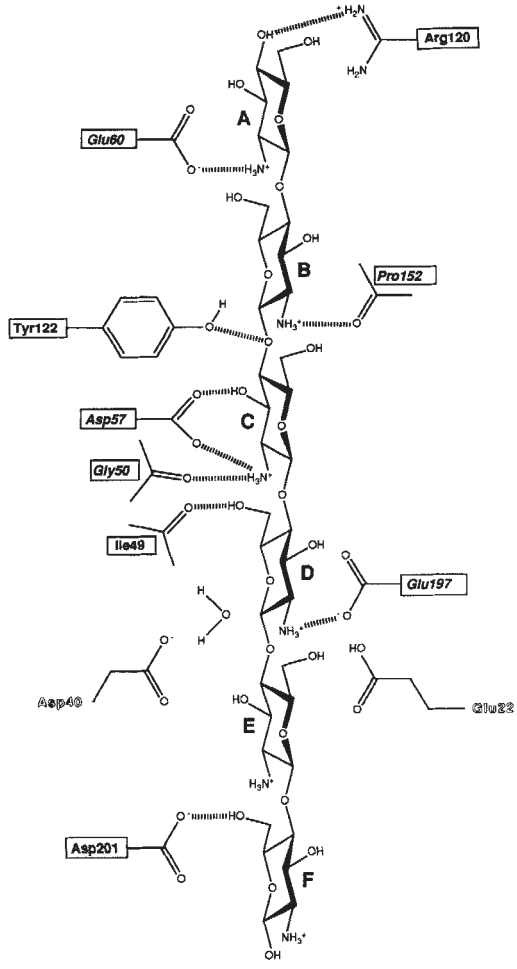

Fig. 6 Schematic representation of the potential interactions between chitosanase and a modelled chitosan hexamer. Residues numbered in italic type appear to confer specificity for the glucosamine polysaccharide, while those numbered in plain type make contacts appropriate for binding common glucose derivatives. The relative positions of a catalytic water and of the putative catalytic residues Glu 22 and Asp 40 are indicated.

The distance observed between Asp 40 and the modelled D sugar's C1 carbon is similar to the spacing observed between Glu 89 of barley chitinase and its model substrate. As seen in chitosanase, the distance between the two chitinase active site carboxylates is also fairly long (11 Å). To bring the acid closer to the D–E glycosidic bond, a conformational change must occur on substrate binding. Such a change seems to occur in barley chitinase; crystals of barley chitinase initially dissolve in the presence of tetraNAG substrate, presumeably due to adopting a conformation incompatible with crystal contacts, and re-form following substrate hydrolysis[21].

The above structural assessment is supported by biochemical evidence that chitosanase is an inverting enzyme (T. Fukamizo, personal communication). Also, site-directed mutagenesis of either Glu 22 or Asp 40 appears to abolish chitosanase's activity in preliminary screens (R.B., unpublished results) confirming the importance of these two residues to the catalytic mechanism of chitosanase.

Methods

Protein preparation and crystallization. *Streptomyces* N174 chitosanase was isolated and prepared as described previously[8]. Crystals were obtained as described previously[13]. Crystal growth was sensitive to vibration, and the largest crystals were obtained when this was controlled.

To combat extreme crystal slippage problems, crystals had to be prepared as follows for data collection. Crystals were fixed by painting with a viscous solution of polystyrene dissolved in benzene. Rapid evaporation of solvent left a crystal and some residual mother liquor embedded in a hard, clear shell of polystyrene glued to the inner wall of the mounting capillary. Data from these crystals merged favorably with incomplete unfixed native data sets and with unfixed-heavy atom data sets. No significant changes in unit cell parameters were observed and evidence of included benzenes was not seen during the refinement, implying that the crystals were essentially unaffected by this treatment.

Data collection and reduction. Three-dimensional diffraction data were collected on a San Diego Multiwire Systems area detector[38] with a Rigaku RU-200 X-ray source operating at 50kV, 100mA with a graphite monochromator. Data were collected from 50 to 2.4 Å using the method of Xuong *et al.*[39] and reduced and evaluated using the University of California, San Diego (UCSD) software system[40].

The presence of a single cysteine in chitosanase suggested that a free thiol might be present. The sole heavy atom derivative was obtained by soaking pre-formed chitosanase crystals in artificial mother liquor consisting of 25% PEG 8000 and 0.2 M potassium phosphate and supplemented with 1 mM $CH_3Hg(C_2H_3O_2)$ for 18 h. Two mercury sites were obtained, establishing the handedness of the molecules and corresponding to single mercury atoms bound at Cys 52 in each of the two molecules in the asymmetric unit of the crystal. Differences in the occupancies of the two supposedly equivalent mercury sites are attributable to the dissimilar environments around Cys 52 caused by non-crystallographic symmetry contacts.

SIRAS phasing. Statistics for X-ray diffraction data collected from native and derivatized chitosanase crystals are summarized in Table 2. Phasing and heavy-atom parameter refinement were performed using the programs PHASEPROG and REFINE obtained from G. Petsko. Isomorphous and anomalous difference data from the methyl mercury derivative were used to calculate a 10–3.0 Å SIRAS map. Solvent flattening performed with the Wang algorithm[41] produced a 10–3 Å electron density map of sufficient quality to build a significant portion of the backbones of both molecules in the asymmetric unit using the programs TOM and FRODO[42].

These models were used to identify an approximate non-crystallographic two-fold operator, allowing map averaging across the two-fold operator using the method of Bricogne[43]. This operator matched fairly minor peaks

Table 2 Crystallographic data

Space group: $P2_1$ (a=56.3 , b=59.3 , c=85.4 Å, β=96.2°)

Streptomyces N174 chitosanase		Native	$CH_3Hg(CH_3O_2)$
No. of observations		121,478	104,156
No. of unique observations		21,903	29,288
Completeness (%)		98.70	91.08
Resolution limit (Å)		2.40	2.68
R_{merge} (%)[1]		8.85	6.04
$R_{crystallographic}$ (%)[2]		18.09	
R_{free} (%)		23.60	
$R_{working}$ (%)		17.48	
R.m.s. deviations from			
ideal bond lengths (Å)	0.016		
ideal bond angles	3.118°		
Mean fractional isomorphous change (%)			17.78

Phasing power[3]	d_{min} (Å)	Phasing power	*Anom*
	6.7	4.3	1.7
	5.5	4.3	1.7
	4.7	3.5	1.3
	4.2	2.7	1.3
	3.9	2.6	0.8
	3.6	2.5	1.0
	3.4	2.4	0.8
	3.2	2.5	0.8
	3.0	2.4	0.6

	Heavy-atom sites (fractional coordinates)			
$CH_3Hg(C_2H_3O_2)$	*X*	*Y*	*Z*	Occupancy (arbitrary units)
1	0.201	0.000	0.084	0.427
2	0.986	0.252	0.316	0.321

Mean figure of merit following solvent flattening = 0.80

[1] $R_{merge}=\Sigma_i|I_i-\langle I_i\rangle| / \Sigma_i \langle I_i\rangle$ where I_i is the intensity of an individual reflection and $\langle I_i\rangle$ is the mean intensity of that reflection. Friedel mates were merged in the native data set and unmerged in the derivative data set.

[2] $R_{crystallographic}=\Sigma |F_{obs,nat}-F_{calc}| / \Sigma |F_{obs,nat}|$

[3] Phasing power=$\langle f_h \rangle/\langle \varepsilon \rangle$, $\langle f_h'' \rangle/\langle \varepsilon'' \rangle$.

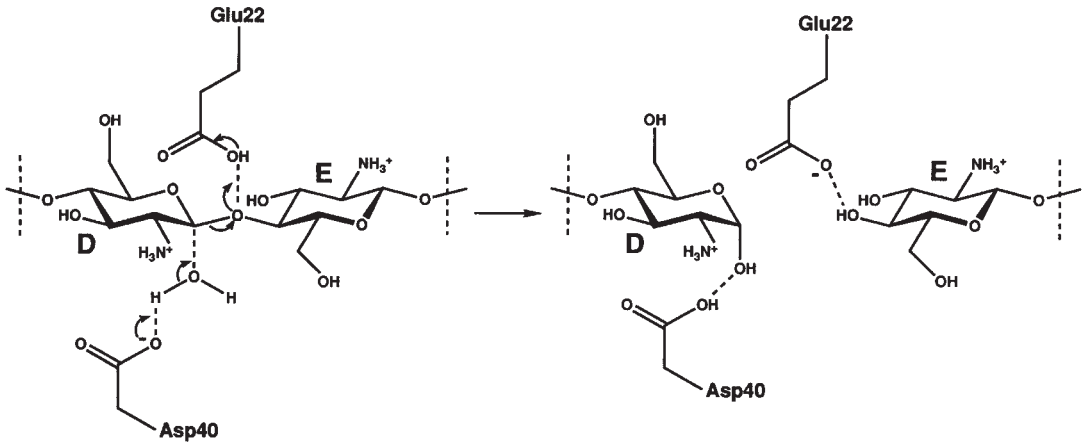

Fig. 7 A postulated single-displacement reaction mechanism of chitosanase.

from a rotation function search[44]. The operator was later improved by rigid-body refinement using CORELS[45] and FRODO real-space refinement, and eventually by X-PLOR[46]. However, because of the apparent inequality of the two chitosanase molecules (the SIRAS/solvent-flattening-phased electron density of the two molecules could not be directly superimposed), the operator was not used for phase improvement by iterative symmetry averaging, but instead served only as a guide for resolving electron-density map ambiguities.

Structure refinement. Refinement proceeded by sequential rounds consisting of hand rebuilding into no electron density (NED) maps and OMIT $2\boldsymbol{F}_o$-$\boldsymbol{F}_c$ maps followed by simulated annealing refinement with X-PLOR[47,48]. NED maps, calculated by an in-house program NEDFFT, are loosely analogous to OMIT maps, but are systematically created for the entire unit cell. To generate NED maps, the asymmetric unit is divided into at least 10 slabs. The starting electron density in one slab is set to zero, along with bordering map sections, and the electron density in the resultant unit cell is back-transformed to produce new calculated structure factors ($\boldsymbol{F}_{calc'}$) and phases. These phases are combined with $|2\bullet\omega\bullet|\boldsymbol{F}_{obs,nat}|-|\boldsymbol{F}_{calc'}||$ structure factor amplitudes, where ω is the Sim weight[48], to calculate a slab of density corresponding to the slab that was initially zeroed but containing less model bias. This process is repeated on consecutive slabs, which are then assembled to produce the complete NED map. By rebuilding the model into NED maps, model-induced phase bias is removed at each round of refinement. Also, as phases improve with refinement, NED maps become strong indicators of model error[49].

Eighteen rounds of refinement were performed. Each included simulated annealing using terms to the resolution limit of that round. Four rounds of energy minimization refinement followed the final simulated annealing refinement round. Water molecules with good geometry, difference map electron density and NED map electron density were included at 2.5 Å resolution. The two molecules in the asymmetric unit were refined initially imposing non-crystallographic symmetry restraints. When the number of reflections included in the refinement provided sufficient overdeterminacy (at 2.6 Å resolution), the two molecules were refined independently. Coordinates of the refined 2.4 Å structure of chitosanase have been submitted to the Brookhaven protein data bank; accession number 1CHK.

Chitosan hexasaccharide model building. Coordinates were available for the trisaccharide NAM-NAG-NAM as solved crystallographically in the active site of HEWL[23] (9LYZ) as well as for the tetra-N-acetyl-glucosamine-δ-lactone crystallographically determined in the HEWL active site[24]. A hexa-β-(1,4)-D-glucosamine molecule was built based upon the tri- and tetra-saccharide models and positioned into the putative N174 chitosanase active site by the alignment of structurally conserved core residues of HEWL with those of N174 chitosanase (fitting chitosanase residues 12–22, 45–51 and 110–119 with HEWL residues 25–35, 52–58 and 91–100; r.m.s. deviation for 28 Cα positions=1.1 Å). The model position was hand adjusted to maximize complementary enzyme-substrate contacts. Positional energy refinement was performed upon the chitosanase-hexaglucosamine model with X-PLOR. The protein backbone was held fixed during the refinement. Electrostatic modeling was performed with the program GRASP, including only ionizable atoms[50].

Received 2 June; accepted 4 December 1995.

Acknowledgements
We are grateful to Elizabeth Goldsmith for generously allowing us to collect a data set on the Southwestern Medical Center diffraction apparatus. This work was supported by grants from the National Institutes of Health, the Foundation for Research and the Welch Foundation. Work at Sherbrooke University was supported by grants from the Natural Sciences and Engineering Council of Canada and from Les Fonds pour la Formation de Chercheurs at l'Aide a la Recherche du Gouvernement du Qubec.

1. Sandford, P. Chitosan: Commercial uses and potential applications. in *Chitin and Chitosan* (eds Skåjk-Bræk, G., Anthonsen, T. & Sandford, P.) 51–69 (Elsevier Applied Science, London, 1989).
2. Bruck, H.M., Nash, G., Foley, F.D. & Pruiti, B.A., Jr. Opportunistic fungal infections of the burn wound with *Phycomyces* and *Aspergillus*. *Arch. Surgery* **102**, 476–482 (1971).
3. Barnicki-Garcia, S. & Nickerson, W.J. Isolation, composition, and structure of cell walls of filamentous and yeast-like forms of *Mucor rouxii*. *Biochim. Biophys. Acta* **58**, 102–119 (1962).
4. El Ghaouth, A., Arul, J., Grenier, J. & Asselin, A. Antifungal activity of chitosan on two postharvest pathogens of strawberry fruits. *Phytopathology* **82**, 398–402 (1992).
5. Hadwiger, L.A., Fristensky, B. & Riggleman, R.C. in *Chitin, Chitosan, and Related Enzymes* (ed. Zikakis, J. P.) 291–302 (Academic Press, Orlando, 1984).
6. Davis, B. & Eveleigh, D.E. in *Chitin, Chitosan, and Related Enzymes* (ed. Zikakis, J. P.) 291-302 (Academic Press, Orlando, 1984).
7. El Ouakfaoui, S. & Asselin, A. Diversity of chitosanase activity in cucumber. *Plant Science* **85**, 33–41 (1992).
8. Boucher, I., Dupuy, A., Vidal, P., Neugebauer, W.A. & Brzezinski, R. Purification and characterization of a chitosanase from *Streptomyces* N174. *Appl. Microb. Biotechnol.* **38**, 188–193 (1992).
9. Fink, D., Boucher, I., Denis, F. & Brzezinski, R. Cloning and expression in *Streptomyces lividans* of a chitosanase-encoding gene from the actinomycete *Kitasatosporia* N174 isolated from soil. *Biotech. Lett.* **13**, 845–850 (1991).
10. Masson, J.-Y., Denis, F. & Brzezinski, R. Primary sequence of the chitosanase from *Streptomyces sp.* strain N174 and comparison with other endoglycosidases. *Gene* **140**, 103–107 (1994).
11. Henrissat, B. & Bairoch, A. New families in the classification of glycosyl hydrolases based on amino acid sequence similarities. *Biochem. J.* **293**, 781–788 (1993).
12. Ando, A., Noguchi, K., Yanagi, M., Shinoyama, H., Kagawa, Y., Hirata, H., Yabuki, M. & Fujii, T. Primary structure of chitosanase produced by *Bacillus circulans* MH-K1. *J. Gen. Appl. Microbiol.* **38**, 135–144 (1992).
13. Marcotte, E., Hart, P.J., Boucher, I., Brzezinski, R. & Robertus, J. D. Crystallization of a chitosanase from *Streptomyces* N174. *J. Molec. Biol.* **232**, 995–996 (1993).
14. Lüthy, R., Bowie, J.U. & Eisenberg, D. Assessment of protein models with three-dimensional profiles. *Nature* **356**, 83–85 (1992).
15. Matthews, B.W. & Remington, S.J. The three dimensional structure of the lysozyme from bacteriophage T4. *Proc. Natl. Acac. Sci. U.S.A.* **71**, 4178–4182 (1974).
16. Rossmann, M.G. & Argos, P. Exploring structural homology of proteins. *J. Molec. Biol.* **105**, 75–96 (1976).
17. Matthews, B.W., Grütter, M.G., Anderson, W.F., & Remington, S.J. Common precursor of lysozymes of hen egg-white and bacteriophage T4. *Nature* **290**, 334–335 (1981).
18. Grütter, M.G., Weaver, L.H. & Matthews, B.W. Goose lysozyme structure: an evolutionary link between hen and bacteriophage lysozymes? *Nature* **303**, 828–831 (1983).
19. Hart, P.J., Monzingo, A.F., Ready, M.P., Ernst, S.R. & Robertus, J.D. Crystal structure of an endochitinase from *Hordeum vulgare* L. seeds. *J. Molec. Biol.* **229**, 189–193 (1993).
20. Holm, L. & Sander, C. Structural similarity of plant chitinase and lysozymes from animals and phage. *FEBS Lett.* **340**, 129–132 (1994).
21. Hart, P.J., Pfluger, H.D., Monzingo, A.F., Hollis, T. & Robertus, J.D. The refined crystal structure of an endochitinase from *Hordeum vulgare* L. seeds at 1.8 Å resolution. *J. Molec. Biol.* **248**, 402–413 (1995).
22. Monzingo, A.F., Marcotte, E.M., Hart, P.J. & Robertus, J.D. Chitinase, chitosanases, and lysozymes can be divided into procaryotic and eukaryotic families sharing a conserved core. *Nature Struct. Biol.* **3**, 133–140 (1996).
23. Kelly, J.A., Sielecki, A.R., Sykes, BD., James, M.N.G. & Phillips, D.C. X-ray crystallography of the binding of the bacterial cell wall trisaccharide NAM-NAG-NAM to lysozyme. *Nature* **282**, 875–878 (1979).
24. Ford, L.O., Johnson, L.N., Machin, P.A., Phillips, D.C. & Tjian, R. Crystal structure of a lysozyme-tetrasaccharide lactone complex. *J. Molec. Biol.* **88**, 349–371 (1974).
25. Blake, C.C.F., Koenig, D.F., Mair, G.A., North, A.C.T., Phillips, D.C. & Sarma, V.R. Structure of hen egg-white lysozyme. *Nature* **206**, 757–761 (1965).
26. Imoto, I., Johnson, L.N., Machin, P.A., Phillips, D.C. & Rupley, J.A. in *The Enzymes* Vol. 7 (ed. Boyer, P.) 665–868 (Academic Press, New York, 1972).
27. Matthews, B.W., Remington, S.J., Grütter, M.G. & Anderson, W.F. Relation between hen egg white lysozyme and bacteriophage T4 lysozyme: Evolutionary implications. *J. Molec. Biol.* **147**, 545–558 (1981).
28. Bennet, A.J. & Sinnott, M.L. Complete kinetic isotope effect description of transition states for acid-catalyzed hydrolyses of methyl α- and β-glucopyranosides. *J. Am. Chem. Soc.* **108**, 72–87 (1986).
29. Amyes, T.L. & Jencks, W.P. Lifetimes of oxocarbenium ions in aqueous solution from common ion inhibition of the solvolysis of α-azido ethers by added azide ion. *J. Am. Chem. Soc.* **111**, 78–88 (1989).
30. Withers, S.G., Warren, R.A.J., Street, I.P., Rupitz, K., Kempton, J.B. & Aebersold, R. Unequivocal demonstration of the involvement of a glutamate residue as a nucleophile in the mechanism of a "retaining" glycosidase. *J. Am. Chem. Soc.* **112**, 5887–5889 (1990).
31. Sinnott, M.L. Catalytic mechanisms of enzymic glycosyl transfer. *Chem. Rev.* **90**, 1171–1202 (1990).
32. Kuroki, R., Weaver, L.H. & Matthews, B.W. A covalent enzyme-substrate intermediate with saccharide distortion in a mutant T4 lysozyme. *Science* **262**, 2030–2033 (1993).
33. Fukamizo, T., Koga, D. & Goto, S. Comparative biochemistry of chitinases - anomeric form of the reaction products. *Biosci. Biotech. Biochem.* **59**, 311–313 (1995).
34. Wang, Q., Graham, R.W., Trimbur, D., Warren, R.A.J. & Withers, S.G. Changing enzymatic reaction mechanisms by mutagenesis: conversion of a retaining glucosidase to an inverting enzyme. *J. Am. Chem. Soc.* **116**, 11594–11595 (1994).
35. McCarter, J.D. & Withers, S.G. Mechanisms of enzymatic glycoside hydrolysis. *Curr. Op. Struct. Biol.* **4**, 885–892 (1994).
36. Hadfield, A.T *et al.* Crystal structure of the mutant D52S hen egg white lysozyme with an oligosaccharide product. *J. Molec. Biol.* **243**, 856–872 (1994).
37. Weaver, L.H., Grütter, M.G. & Matthews, B.W. The refined structures of goose lysozyme and its complex with a bound trisaccharide show the goose-type lysozymes lack a catalytic aspartate residue. *J. Molec. Biol.* **245**, 54–68 (1995).
38. Hamlin, R. Multiwire area X-ray diffractometers. *Meth. Enzymol.* **114**, 416–452 (1985).
39. Xuong, N.H., Nielson, C., Hamlin, R. & Anderson, D. Strategies for data collection from protein crystals using a multiwire counter area detector diffractometer. *J. Appl. Crystallogr.* **18**, 342–350 (1985).
40. Howard, A.J., Nielsen, C. & Xuong, N.H. Software for a diffractometer with multiwire area detector. *Methods Enzymol.* **114**, 453–472 (1985).
41. Wang, B.-C. Resolution of phase ambiguity in macromolecular crystallography. *Methods Enzymol.* **115**, 90–112 (1985).
42. Jones, T.A. in *Computational Crystallography* (ed. Sayre, D.) 303–317 (Oxford University, Oxford, 1982).
43. Bricogne, G. Methods and programs for direct-space exploration of geometric redundancies. *Acta Crystallogr.* A **32**, 832–847 (1976).
44. Tanaka, N. Representation of the fast-rotation function in a polar coordinate system. *Acta Crystallogr.* A **33**, 191–193 (1977).
45. Sussman, J.L. Constrained-restrained least squares (CORELS) refinement of proteins and nucleic acids. *Meth. Enzymol.* **115**, 271–302 (1985).
46. Brünger, A.T. in *Crystallographic Computing 4: Techniques and New Technologies* (eds Isaacs, N. W. & Taylor, M. R.) 126–140 (Clarendon Press, Oxford, 1988).
47. Rutenber, E.*et al.* Crystallographic refinement of ricin to 2.5 Å. *Prot. Struct. Funct. Genet.* **10**, 240-250 (1991).
48. Sim, G.A. The distribution of phase angles for structures containing heavy atoms. *Acta. Crystallogr.* **12**, 813–815 (1959).
49. Monzingo, A.F., Collins, E.J., Ernst, S.R., Irvin, J.D. & Robertus, J.D. The 2.5 Å structure of pokeweed antiviral protein. *J. Molec. Biol.* **233**, 705–715 (1993).
50. Nicholls, A., Sharp, K. A. & Honig, B. Protein folding and association: Insights from the interfacial and thermodynamic properties of hydrocarbons. *Prot. Struct. Funct. Genet.* **11**, 281–293 (1991).
51. Kraulis, P.J. MOLSCRIPT: A program to produce both detailed and schematic plots of protein structures. *J. Appl. Crystallogr.* **24**, 946–950 (1991).